Table 1 Data used in this study

Comb. No.	DMSP satellites	Data period	Length (mon)	Morning Eq. Crossing (LST)
	F08	Jul '87 - Feb '90*	31	0615
	F11	Jan '92 - Dec '95	48	0501-0629 (0545 nominal)
	F13	Jan '96 - Feb '98	26	0543
	F10	Jan '91 - Nov '97	83	0742-1031 (0900 nominal)
1	F08/11/13	Jul '87 - Feb '90* & Jan '92 - Feb '98	95	0600 (nominal)
2	F08/11/13/10 (all the data)	Jul '87 - Feb '90* & Jan '91 - Feb '98	107	0600/0900 (nominal)
3	F08/11/13/10 (common period)	Jan '92 – Nov '97	71	0600/0900 (nominal)

* except Dec '87

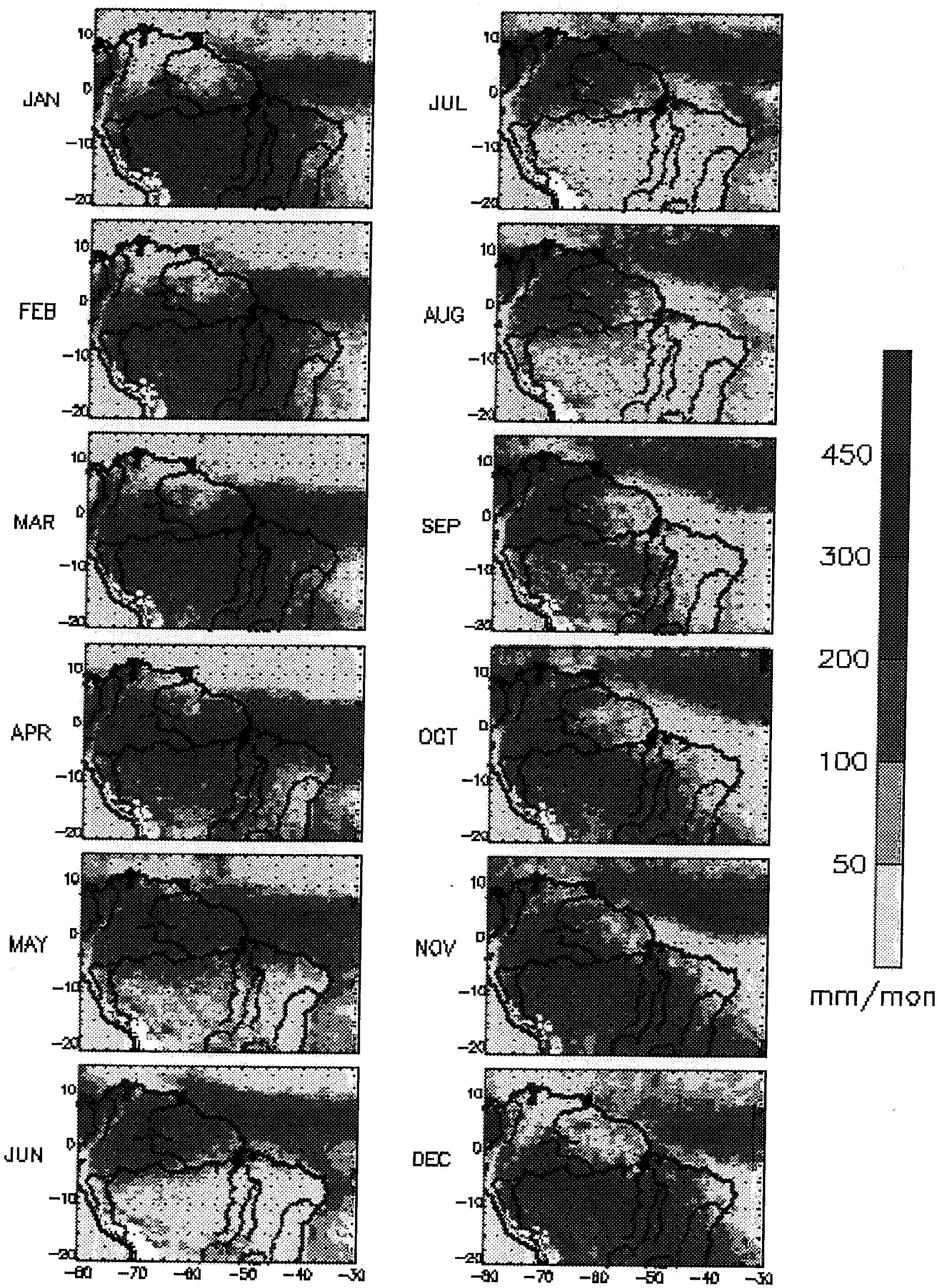
JAN
FEB
MAR
APR
MAY
JUN
JUL
AUG
SEP
OCT
NOV
DEC
10
0
-10
-20
-80
-70
-60
-50
-40
-30
450
300
200
100
50
mm/mon

Figure 2

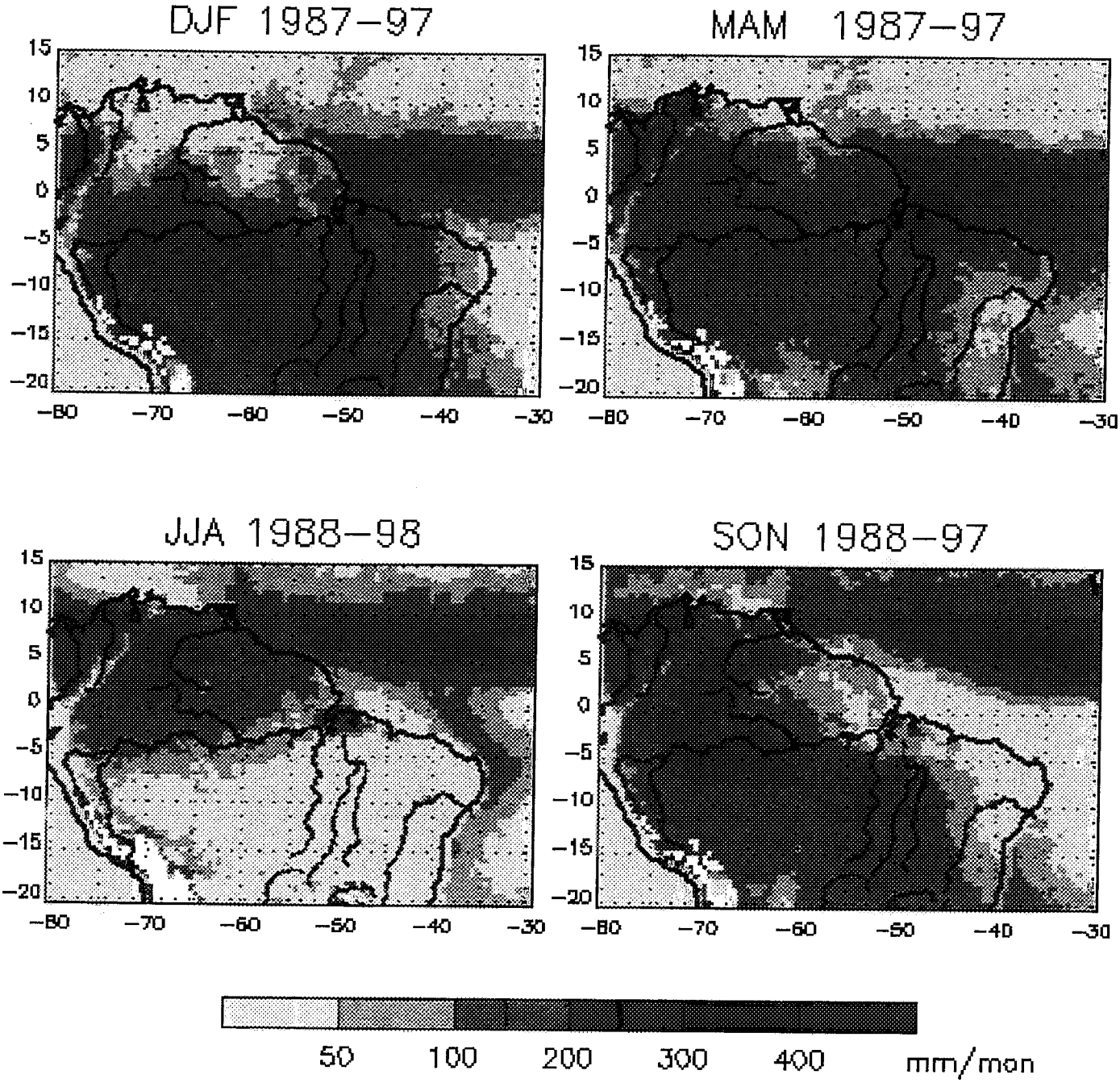
DJF 1987–97
MAM 1987–97
JJA 1988–98
SON 1988–97
15
10
5
0
–5
–10
–15
–20
–80
–70
–60
–50
–40
–30
50
100
200
300
400
mm/mon

Figure 3

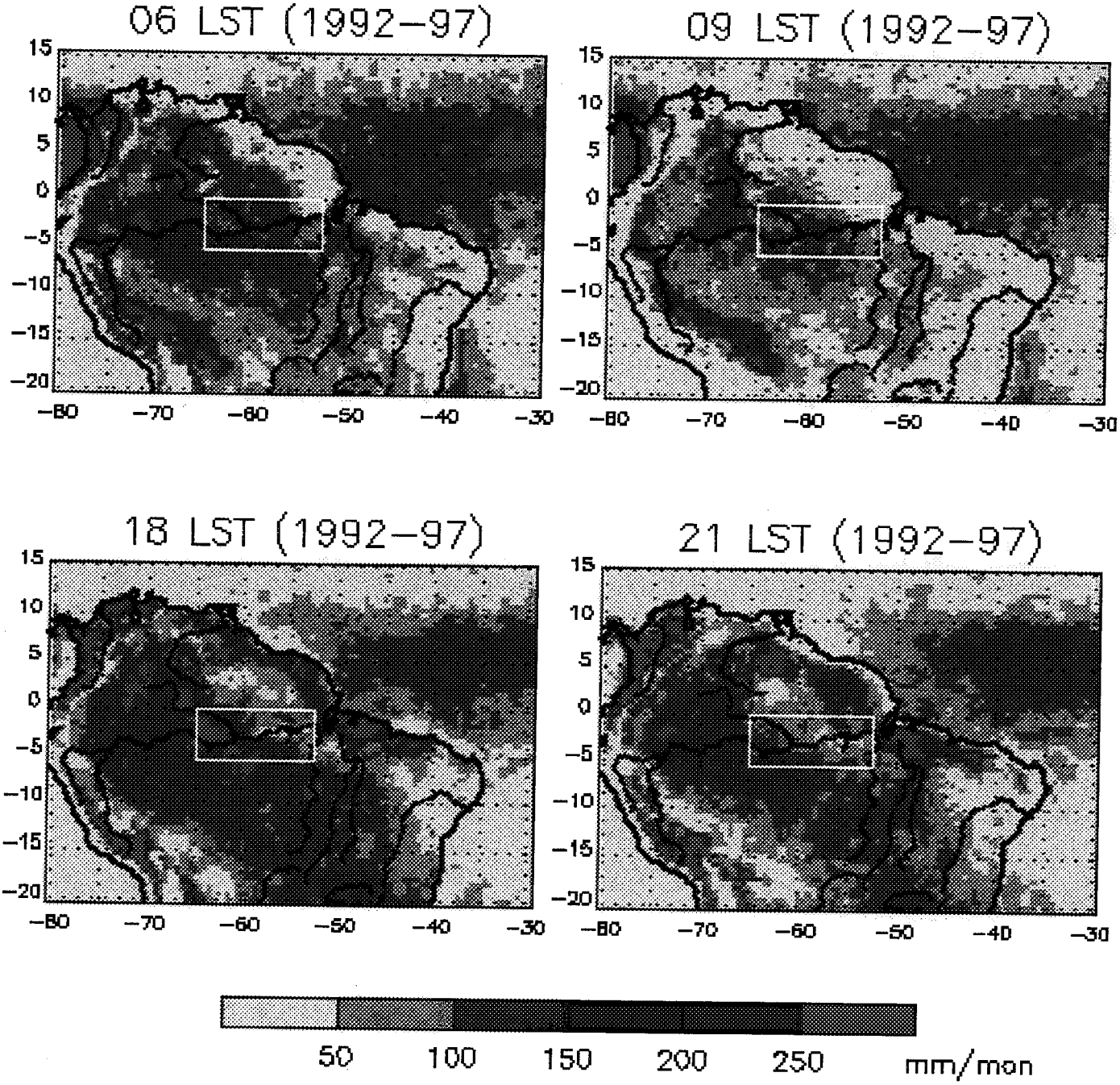
06 LST (1992–97)
09 LST (1992–97)
18 LST (1992–97)
21 LST (1992–97)
15
10
5
0
−5
−10
−15
−20
−80
−70
−60
−50
−40
−30
50
100
150
200
250
mm/mon

Figure 4

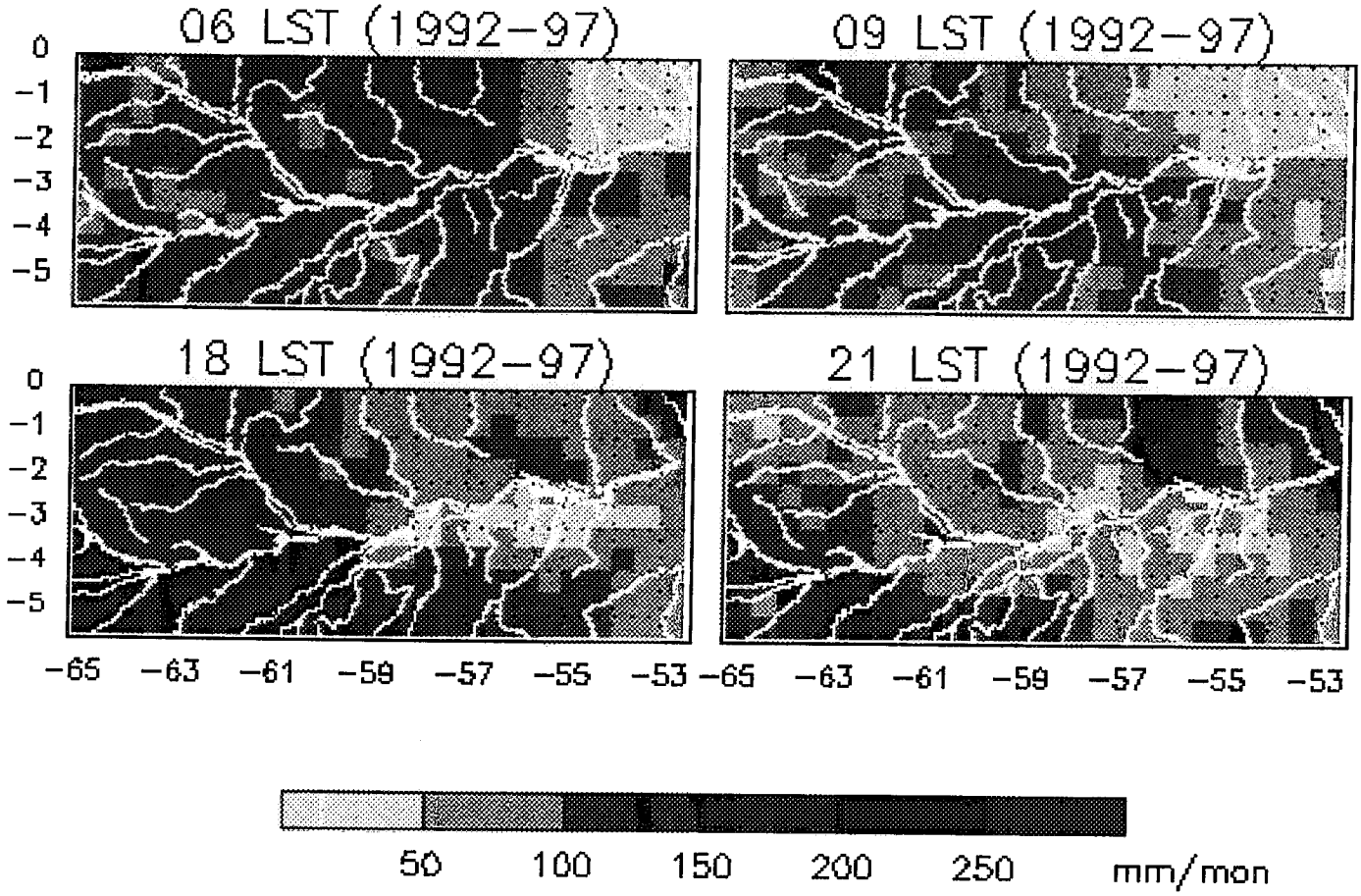
06 LST (1992–97)
09 LST (1992–97)
18 LST (1992–97)
21 LST (1992–97)
0
−1
−2
−3
−4
−5
−65 −63 −61 −59 −57 −55 −53
50 100 150 200 250 mm/mon

Figure 5

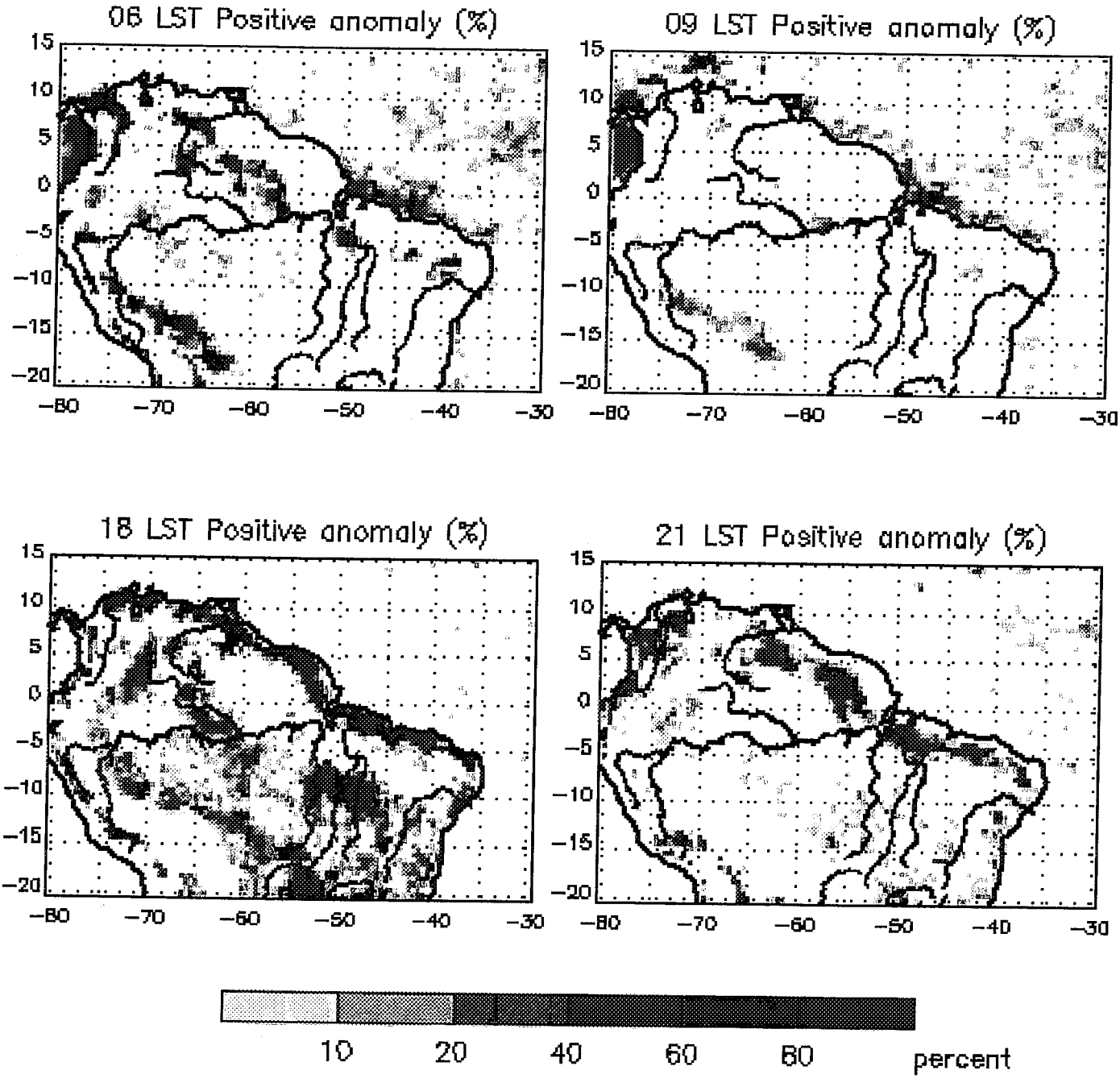
06 LST Positive anomaly (%)
09 LST Positive anomaly (%)
18 LST Positive anomaly (%)
21 LST Positive anomaly (%)
15
10
5
0
-5
-10
-15
-20
-80
-70
-60
-50
-40
-30
10
20
40
60
80
percent

Figure 6

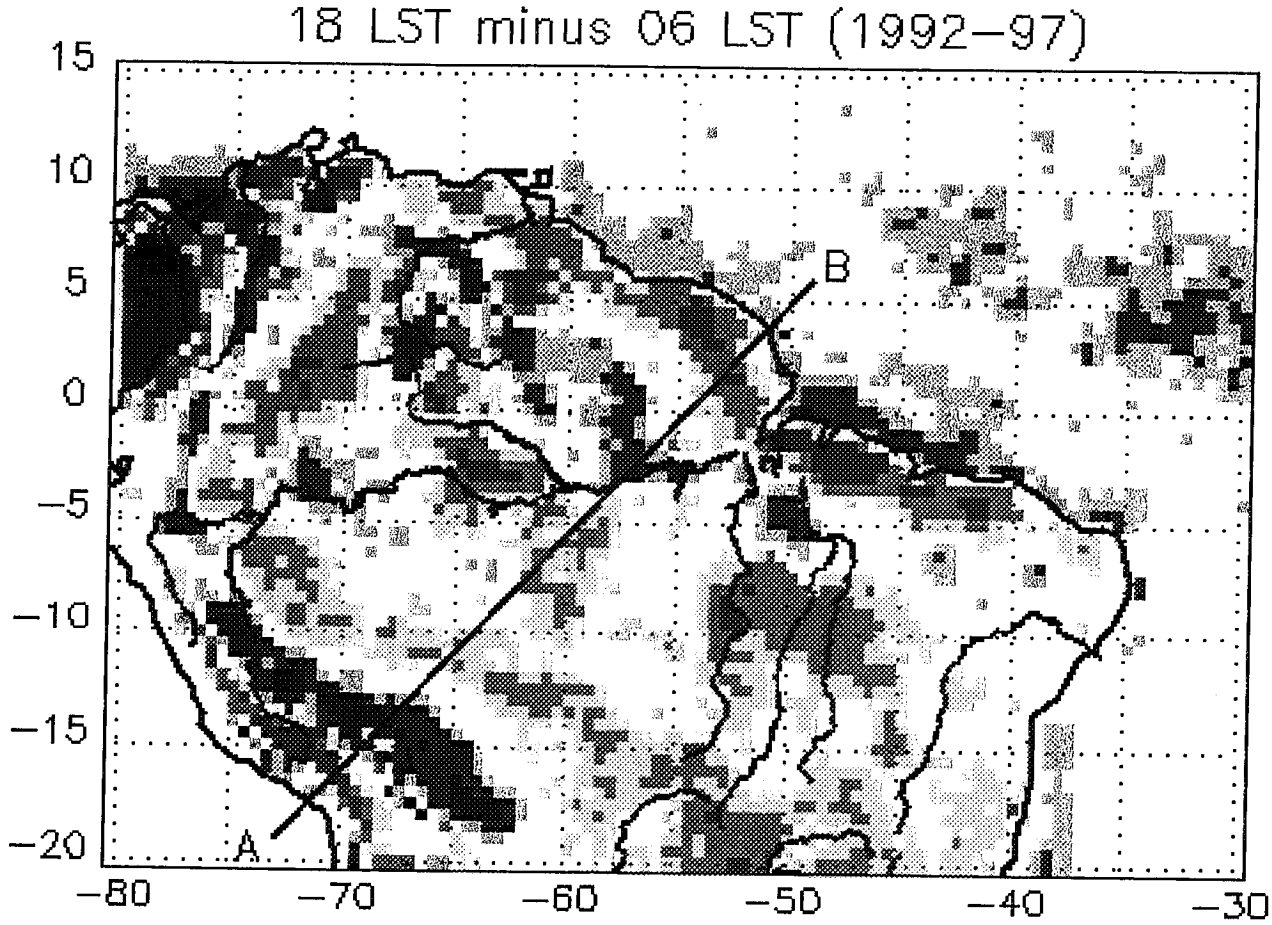
18 LST minus 06 LST (1992–97)
15
10
5
0
−5
−10
−15
−20
A
B
−80
−70
−60
−50
−40
−30

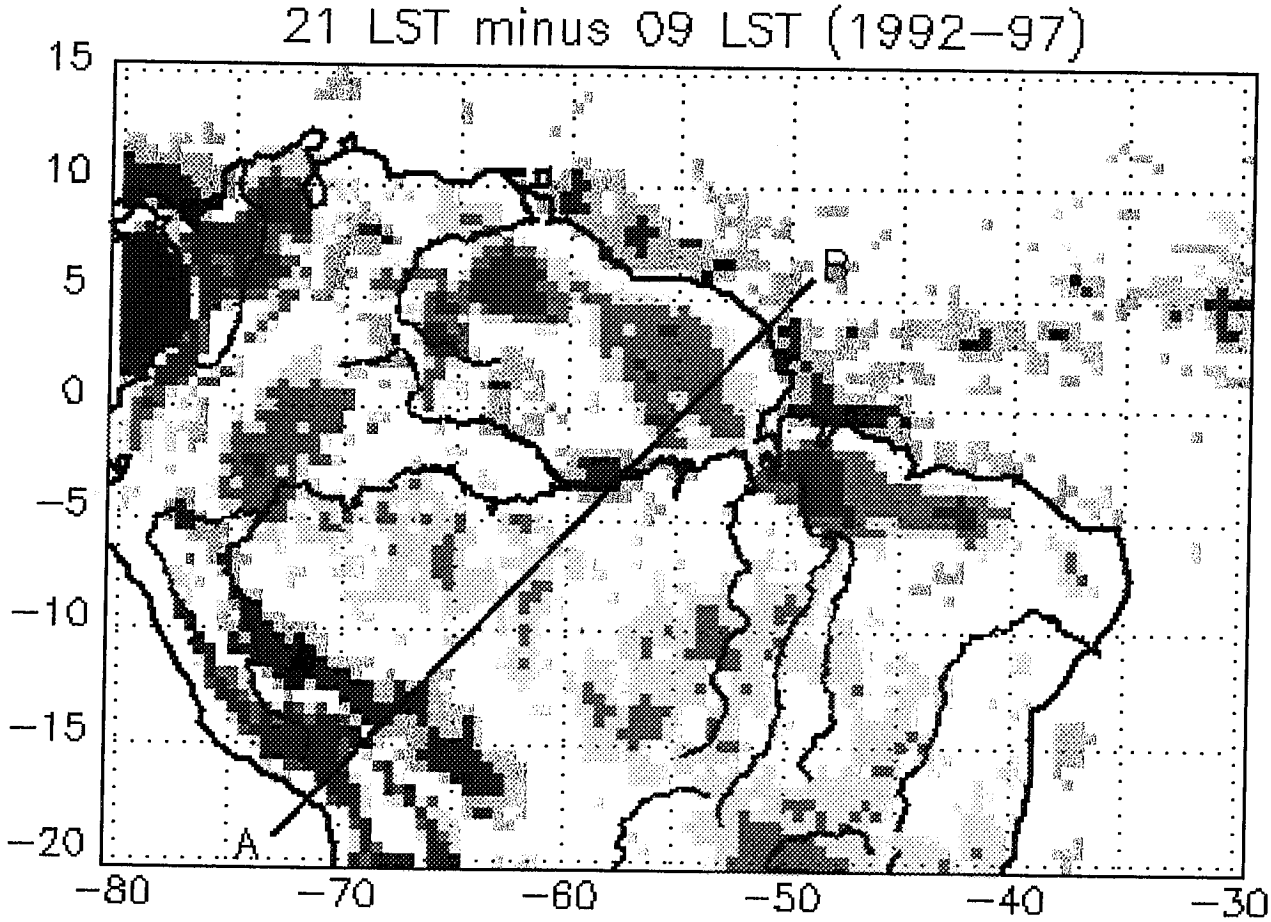
21 LST minus 09 LST (1992–97)
15
10
5
0
−5
−10
−15
−20
A
B
−80
−70
−60
−50
−40
−30

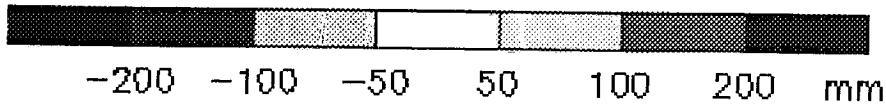
−200
−100
−50
50
100
200
mm/mon

Figure 7

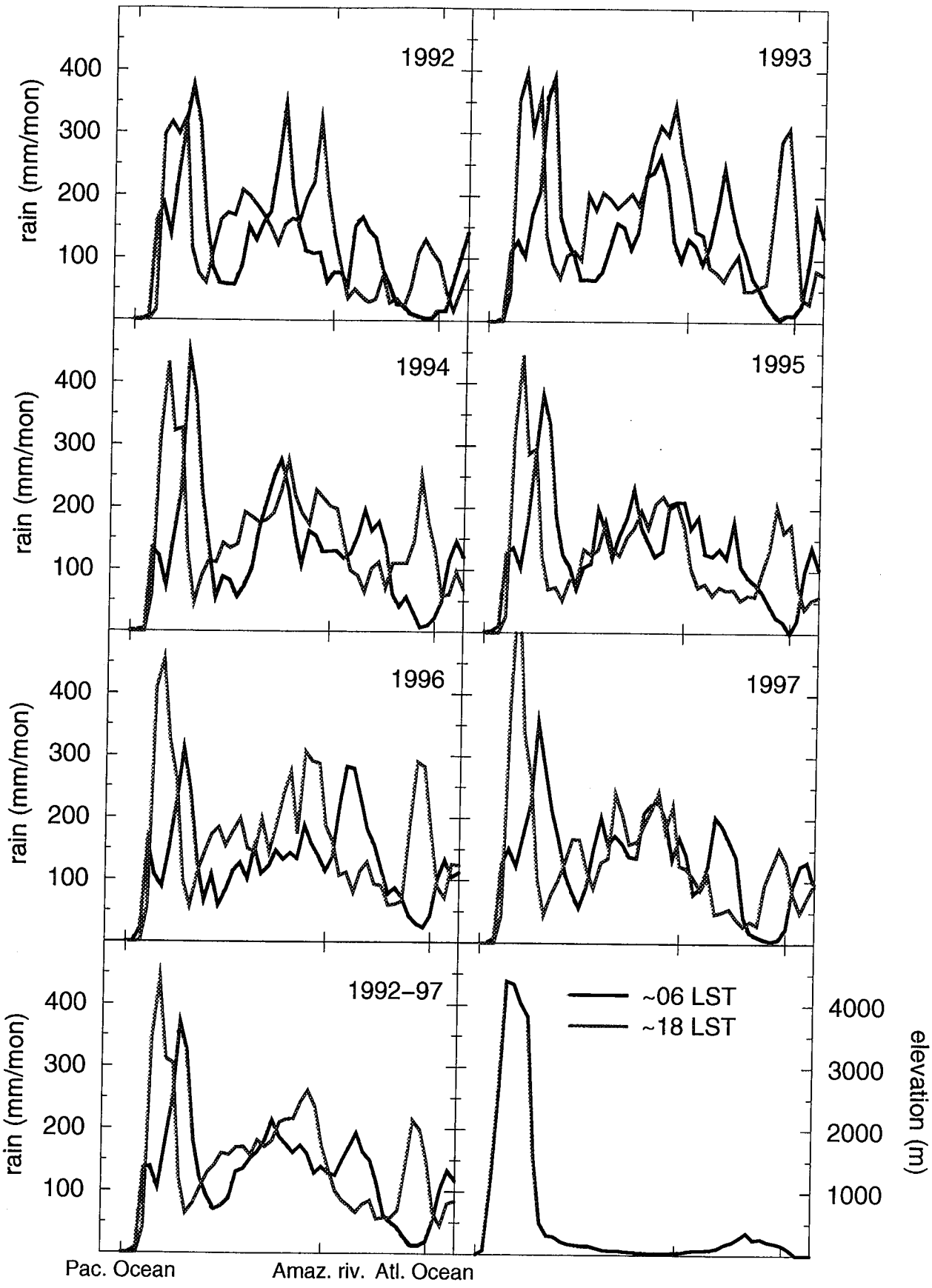
1992
1993
1994
1995
1996
1997
1992–97
rain (mm/mon)
400
300
200
100
~06 LST
~18 LST
4000
3000
2000
1000
elevation (m)
Pac. Ocean
Amaz. riv.
Atl. Ocean

Figure 8

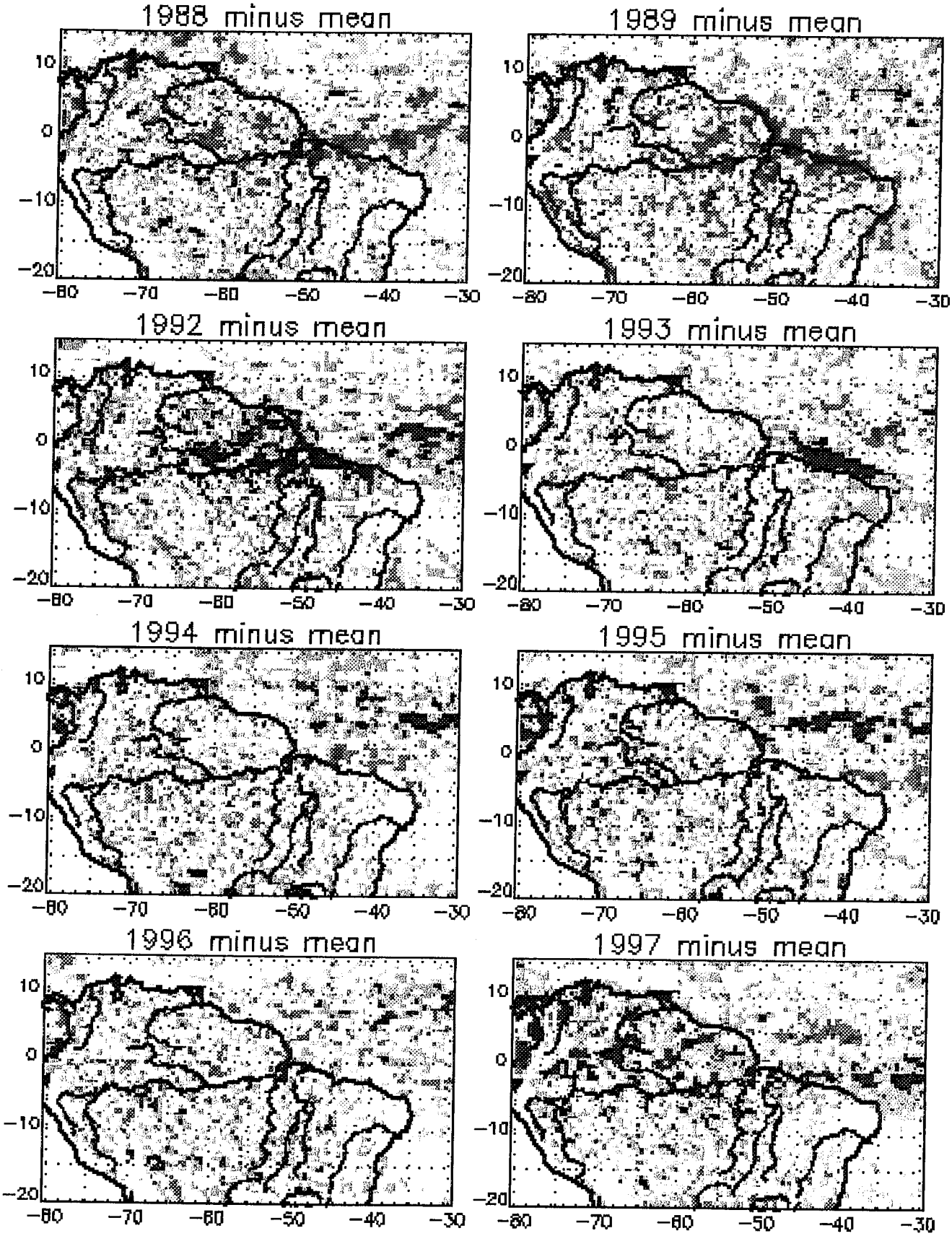
1988 minus mean
1989 minus mean
1992 minus mean
1993 minus mean
1994 minus mean
1995 minus mean
1996 minus mean
1997 minus mean
10
0
−10
−20
−80
−70
−60
−50
−40
−30
−100
−50
−25
25
50
100
mm/mon

Figure 9

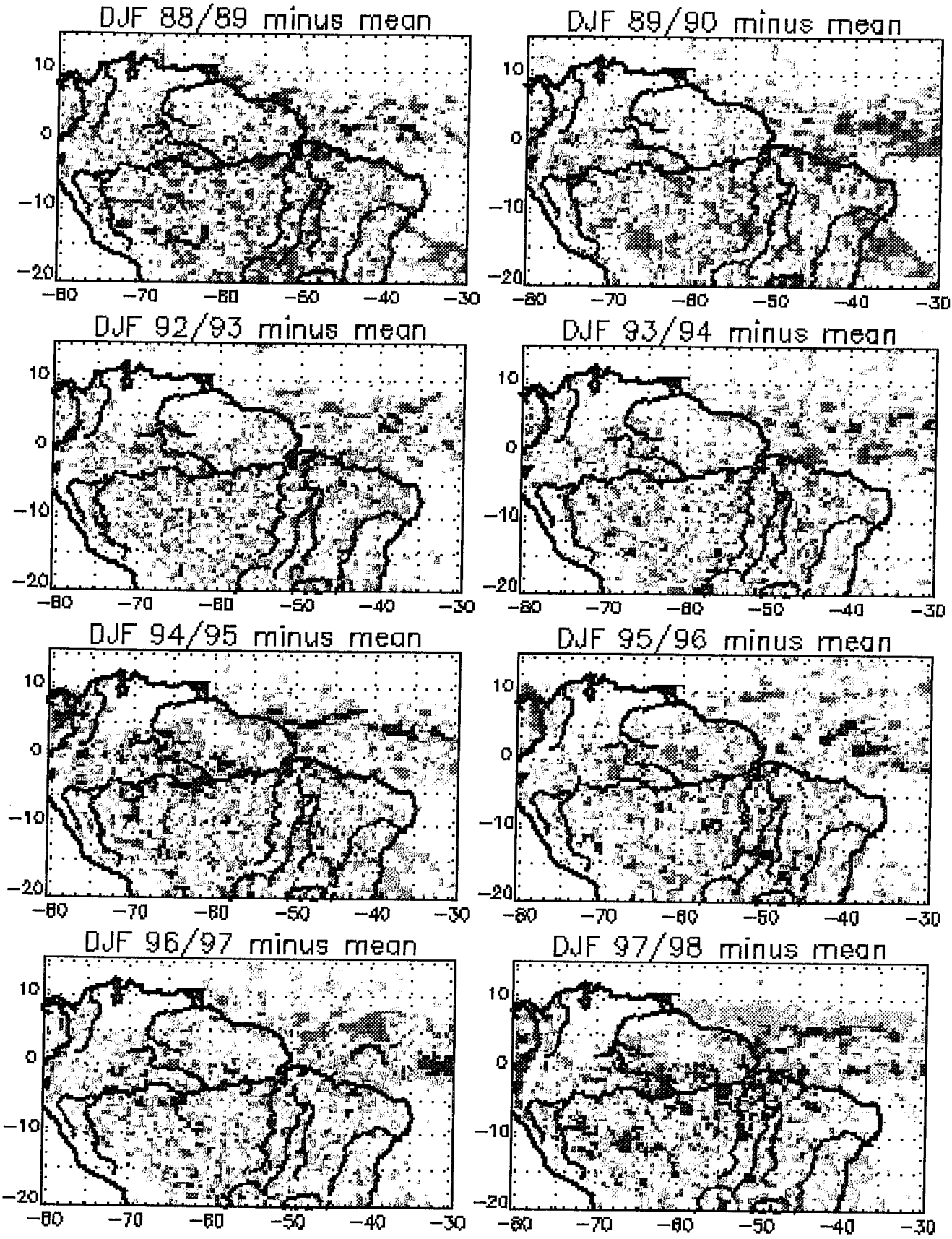
DJF 88/89 minus mean
DJF 89/90 minus mean
DJF 92/93 minus mean
DJF 93/94 minus mean
DJF 94/95 minus mean
DJF 95/96 minus mean
DJF 96/97 minus mean
DJF 97/98 minus mean
10
0
-10
-20
-80
-70
-60
-50
-40
-30
-200
-100
-50
50
100
200
mm/mon

Figure 10

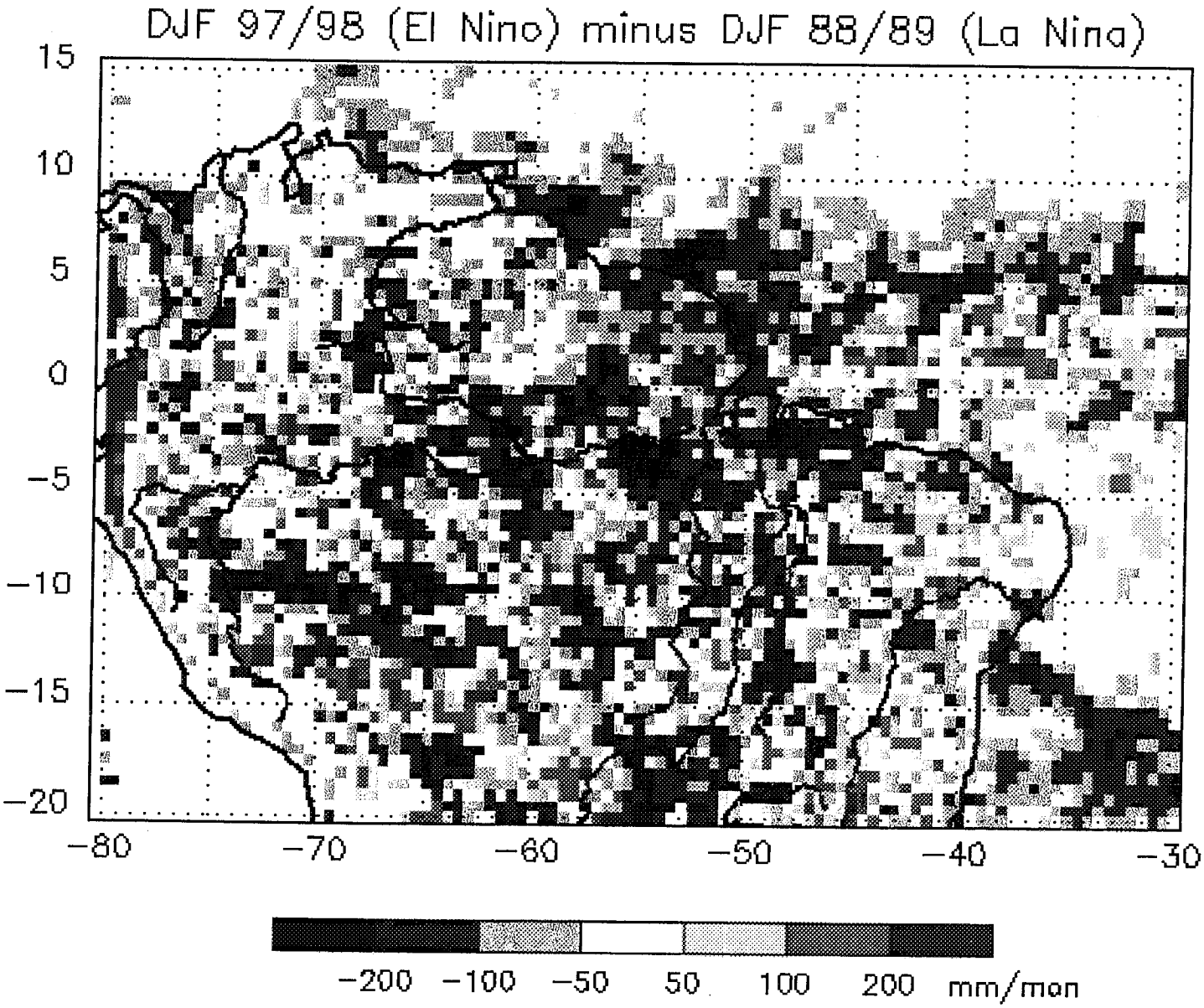
DJF 97/98 (El Nino) minus DJF 88/89 (La Nina)
15
10
5
0
−5
−10
−15
−20
−80
−70
−60
−50
−40
−30
−200
−100
−50
50
100
200
mm/mon

Figure 11

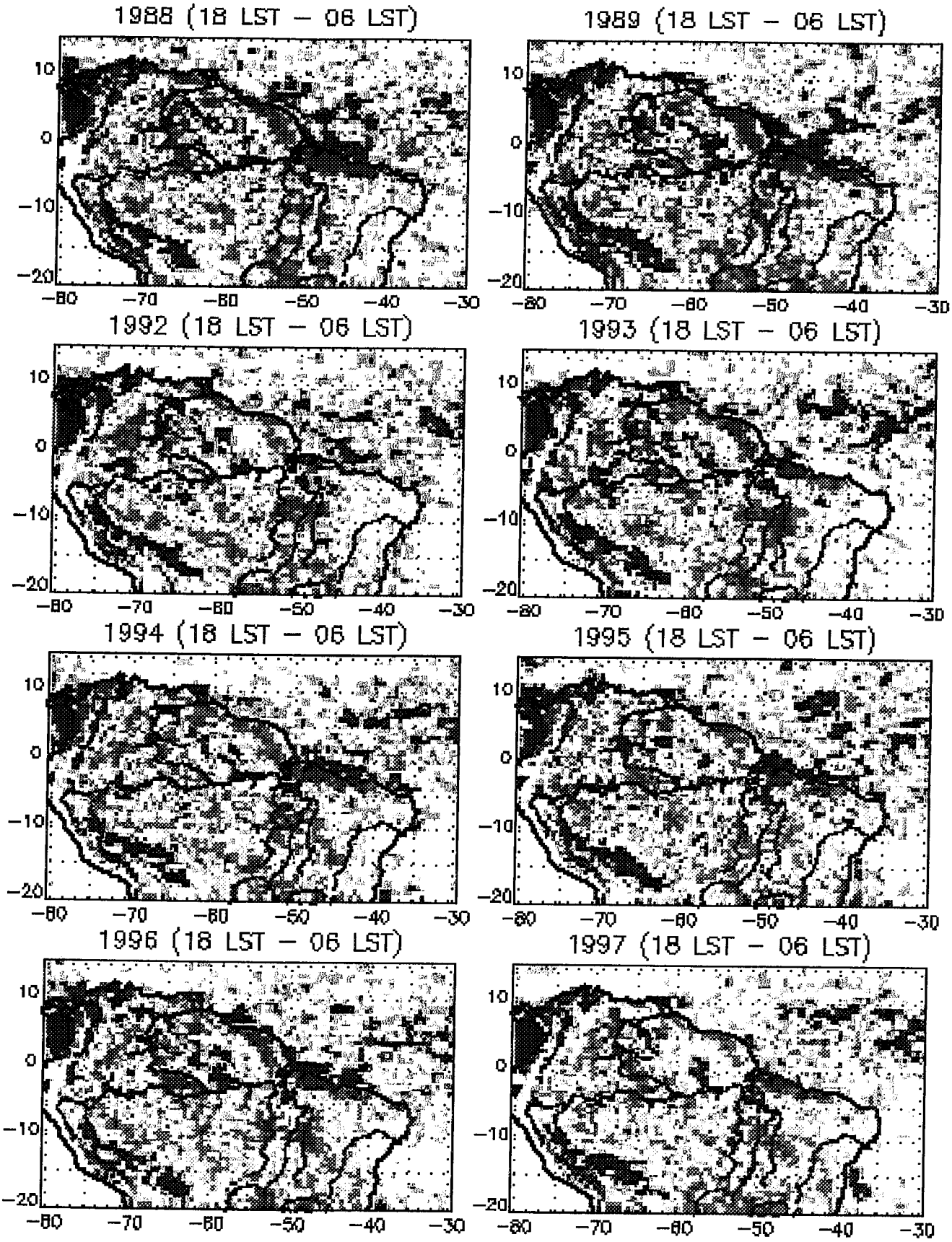
1988 (18 LST − 06 LST)
1989 (18 LST − 06 LST)
1992 (18 LST − 06 LST)
1993 (18 LST − 06 LST)
1994 (18 LST − 06 LST)
1995 (18 LST − 06 LST)
1996 (18 LST − 06 LST)
1997 (18 LST − 06 LST)
10
0
−10
−20
−80
−70
−60
−50
−40
−30
−200 −100 −50 50 100 200 mm/mon

Figure 12

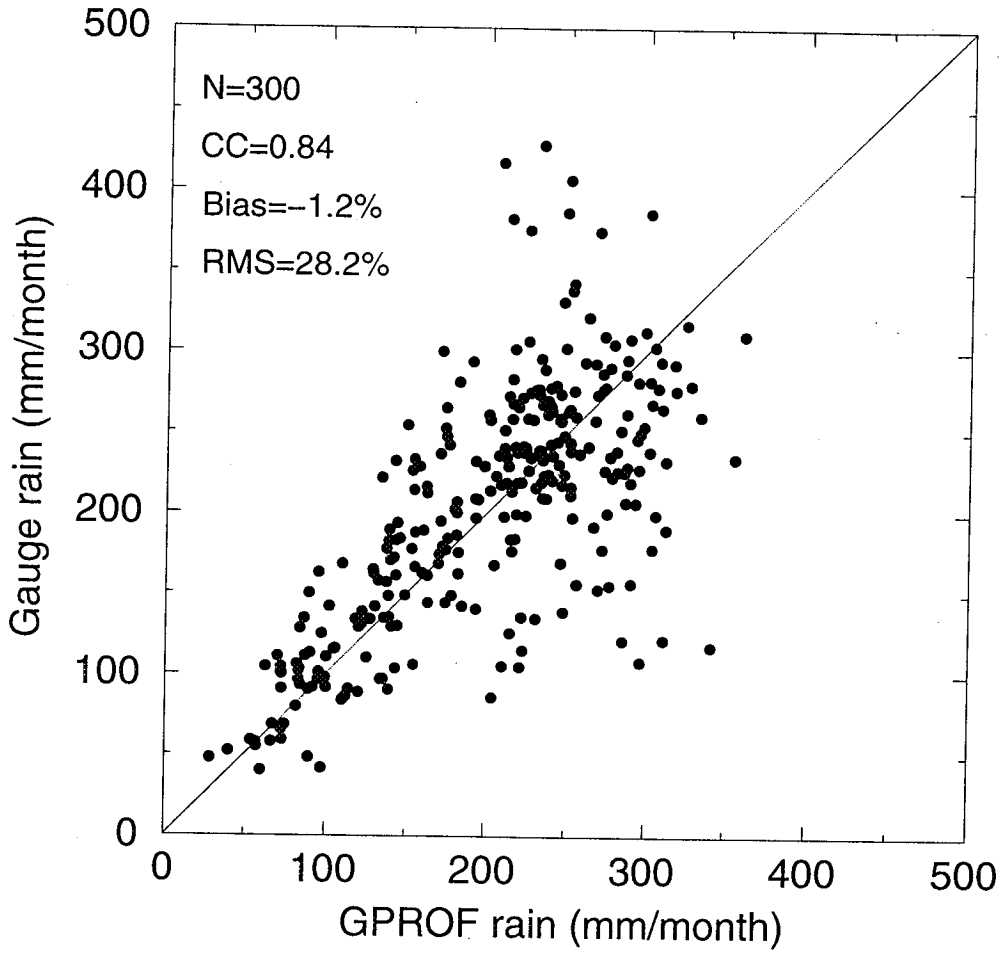
N=300
CC=0.84
Bias=-1.2%
RMS=28.2%
Gauge rain (mm/month)
GPROF rain (mm/month)
0
100
200
300
400
500

Figure 13

National Aeronautics and Space Administration

NASA Scientific and Technical Document Availability Authorization (DAA)

The DAA approval process applies to all forms of published NASA Scientific and Technical Information (STI), whether disseminated in print or electronically. It is to be initiated by the responsible NASA Project Officer, Technical Monitor, author, or other appropriate NASA official for all presentations, reports, papers, and proceedings that contain NASA STI. Explanations are on the back of this form and are presented in greater detail in NPG 2200.2, "Guidelines for Documentation, Approval, and Dissemination of NASA Scientific and Technical Information."

[X] Original
[ ] Modified

I. DOCUMENT/PROJECT IDENTIFICATION

TITLE	AUTHOR(S)
A 10-Year Climatology of Amazonian Rainfall Derived from Passive Microwave Satellite Observations	Andrew J. Negri, Emmanouil N. Anagnostou, and Robert F. Adler
ORIGINATING NASA ORGANIZATION: NASA Goddard Space Flight Center	PERFORMING ORGANIZATION *(If different)*
CONTRACT/GRANT/INTERAGENCY/PROJECT NUMBER(S)	DOCUMENT NUMBER(S) / DOCUMENT DATE

For presentations, documents, or other STI to be externally published (including through electronic media), enter appropriate information on the intended publication such as name, place, and date of conference, periodical, or journal name, or book title and publisher in the next box. These documents must be routed to the NASA Headquarters or Center Export Control Administrator for approval (see Sections III and VIII).

▶ Journal of Applied Meteorology

II. SECURITY CLASSIFICATION

CHECK ONE *(One of the five boxes denoting Security Classification must be checked.)*

[ ] SECRET [ ] SECRET RD [ ] CONFIDENTIAL [ ] CONFIDENTIAL RD [X] UNCLASSIFIED

III. AVAILABILITY CATEGORY

[ ] ITAR [ ] EAR

Export Controlled Document - USML Category /CCL Export Control Classification Number (ECCN) *(Documents marked in this block must have the concurrence/approval of the NASA Headquarters or Center Export Control Administrator (see Section VIII).)*

Confidential Commercial Document *(check appropriate box at left and indicate below the appropriate limitation and expiration)*:

[ ] TRADE SECRET
[ ] SBIR
[ ] COPYRIGHTED

[ ] U.S. Government agencies and U.S. Government agency contractors only
[ ] NASA contractors and U.S. Government only
[ ] U.S. Government agencies only
[ ] NASA personnel and NASA contractors only
[ ] NASA personnel only
[ ] Available only with the approval of issuing office:
[ ] Limited until *(date)*

[X] PUBLICLY AVAILABLE

Publicly available documents must be unclassified, may not be export controlled, may not contain trade secret or confidential commercial data, and should have cleared any applicable patents application process.

IV. DOCUMENT DISCLOSING AN INVENTION

THIS DOCUMENT MAY BE RELEASED ON *(date)*	NASA HQ OR CENTER PATENT OR INTELLECTUAL PROPERTY COUNSEL SIGNATURE	DATE

V. BLANKET RELEASE (OPTIONAL)

[ ] All documents issued under the following contract/grant/project number may be processed as checked in Sections II and III.

[ ] The blanket release authorization granted on *(date)*

[ ] is RESCINDED - Future documents must have individual availability authorizations.

[ ] is MODIFIED - Limitations for all documents processed in the STI system under the blanket release should be changed to conform to blocks as checked in Sections II and III.

PLEASE CONTINUE ON REVERSE SIDE.

VI. AUTHOR/ORIGINATOR VERIFICATION

I HAVE DETERMINED THAT THIS PUBLICATION:

☐ DOES contain export controlled, confidential commercial information, and/or discloses an invention for which a patent has been applied, and the appropriate limitation is checked in Sections III and/or IV.

☒ does NOT contain export controlled, confidential commercial information, nor does it disclose an invention for which a patent has been applied, and may be released as indicated above.

NAME OF AUTHOR/ORIGINATOR	MAIL CODE	SIGNATURE	DATE
Andrew J. Negri	912	Andrew J. Negri	9/25/98

VII. PROJECT OFFICER/TECHNICAL MONITOR/DIVISION CHIEF REVIEW

☐ APPROVED FOR DISTRIBUTION AS MARKED ON REVERSE ☐ NOT APPROVED

NAME OF PROJECT OFFICER OR TECH. MONITOR	MAIL CODE	SIGNATURE	DATE
Franco Einaudi	910	Franco Einaudi	9/28/98

VIII. EXPORT CONTROL REVIEW/CONFIRMATION

☒ Public release is approved ☒ Export controlled limitation is not applicable

☐ Export controlled limitation is approved ☐ Export controlled limitation (ITAR/EAR) marked in Section III is assigned to this document:

USML CATEGORY NUMBER	CCL ECCN NUMBER	HQ OR CENTER EXPORT CONTROL ADMINISTRATOR *(as applicable)*	DATE
N/A	N/A	J. R. Hedgpeth, Code 234	9/29/98

IX. PROGRAM OFFICE OR DELEGATED AUTHORITY REVIEW

☐ APPROVED FOR DISTRIBUTION AS MARKED ON REVERSE ☐ NOT APPROVED

NAME OF PROGRAM OFFICE REPRESENTATIVE	MAIL CODE	SIGNATURE	DATE
Vincent V. Salomonson	900	Vincent V. Salomonson	10/2/98

X. DISPOSITION

THIS FORM, WHEN COMPLETED, IS TO BE SENT TO YOUR CENTER PUBLICATIONS OFFICE

INSTRUCTIONS FOR COMPLETING THE NASA SCIENTIFIC AND TECHNICAL DOCUMENT AVAILABILITY AUTHORIZATION (DAA) FORM

Purpose. This DAA form is used to prescribe the availability and distribution of all NASA-generated and NASA-funded documents containing scientific and technical information (including those distributed via electronic media such as the World Wide Web and CD-ROM).

Requirements. The author/originator must provide either a suitable summary description (title, abstract, etc.) or a completed copy of the document with this form. This form is initiated by the document author/originator and that individual is responsible for recommending/determining the availability/distribution of the document. The author/originator completes Sections I through III, and VI. The author/originator is also responsible for obtaining information and signature in Section IV to the extent the document discloses an invention for which patent protection has been applied. Subsequent to completion of these sections, the author/originator forwards the document to the appropriate Project Manager/Technical Monitor/Division Chief for further review and approval in Section VII, including a re-review of the planned availability and distribution. Once this approval is obtained, the DAA is forwarded to the NASA Headquarters or Center Export Administrator for completion of Section VIII. It is then forwarded for completion of Section IX to the cognizant NASA Headquarters Program Office or Delegated Authority, who provides final review and approval for release of the document as marked.

When to Use This Form. Documents containing STI and intended for presentation or publication (including via electronic media) must be approved in accordance with the NASA STI Procedures and Guidelines (NPG 2200.2). Documents that are to be published in the NASA STI Report Series must be coordinated with the appropriate NASA Headquarters or Center Scientific and Technical Information Office in accordance with NPG 2200.2. Note that information on the Report Documentation Page (if attached) is not to be entered on the DAA except for title, document date, and contract number.

How to Use this Form. Specific guidelines for each section of this form are detailed below.

I. Document/Project Identification. Provide the information requested. If the document is classified, provide instead the security classification of the title and abstract. (Classified information must not be entered on this form). Include RTOP numbers on the Contract/Grant/Interagency/Project Number(s) line. Provide information on presentations or externally published documents as applicable.

II. Security Classification. Enter the applicable security classification for the document. Documents, if classified, will be available only to appropriately cleared personnel having a "need to know."

III. Availability Category for Unclassified Documents. Check the appropriate category or categories.

Export Controlled Document. If the document is subject to export restrictions (see NPG 2200.2, paragraph 4.5.3), the appropriate restriction must be checked, either International Traffic in Arms Regulations (ITAR) or Export Administration Regulations (EAR), and the appropriate United States Munitions List (USML) category or Commerce Control List (CCL), Export Control Classification Number (ECCN) must be cited.

Confidential Commercial Documents (Documents containing Trade Secrets, SBIR documents, and/or Copyrighted information). Check the applicable box (see NPG 2200.2 paragraph 4.5.7). When any of these boxes are checked, also indicate the appropriate limitation and expiration in the list to the right of these restrictions. These limitations refer to the user groups authorized to obtain the document. The limitations apply both to the initial distribution of the documents and the handling of requests for the documents. The limitations will appear on and apply to reproduced copies of the document. Documents limited to NASA personnel should not be made available to onsite contractors. If the Available Only With the Approval of Issuing Office limitation is checked, the NASA Center for AeroSpace Information will provide only bibliographic processing and no initial distribution; CASI will refer all document requests to the issuing office.

Publicly Available Document - Unrestricted Distribution. Check this box if the information in the document may be made available to the general public without restrictions (unrestricted domestic and international distribution). If the document is copyrighted (see paragraph 4.5.7.3 in NPG 2200.2), also check the "Copyrighted" box in this section.

IV. Document Disclosing an Invention. This must be completed when the document contains information that discloses an invention (see NPG 2200.2, paragraph 4.5.9). When this box is checked, an additional appropriate availability category must be checked. Use of this category must be approved by NASA Headquarters or Center Patent Counsel or the Intellectual Property Counsel.

V. Blanket Release (Optional). Complete this optional section whenever subsequent documents produced under the contract, grant, or project are to be given the same distribution and/or availability as described in Sections II and III. More than one contract number or RTOP Number can be entered. This section may also be used to rescind or modify an earlier Blanket Release. All blanket releases must be approved by the Program Office or its designee and concurred with by the Office of Management Systems and Facilities.

VI. Author/Originator Verification. Required for all DAA forms.

VII. Project Officer/Technical Monitor/Division Chief Review. The Project Officer/Technical Monitor/Author or Originator Division Chief or above must sign and date the form. The office code and typed name should be entered.

VIII. Export Control Review/Confirmation. This section is to be completed by the authorized NASA Headquarters or Center Export Control Administrator for all documents.

IX. Program Office or Delegated Authority Review. This section is to be completed by the duly authorized official representing the NASA Headquarters Program Office. Any delegation from NASA Headquarters to a NASA Center in accordance with NPG 2200.2 should be entered here.

X. Disposition. For NASA Center use.

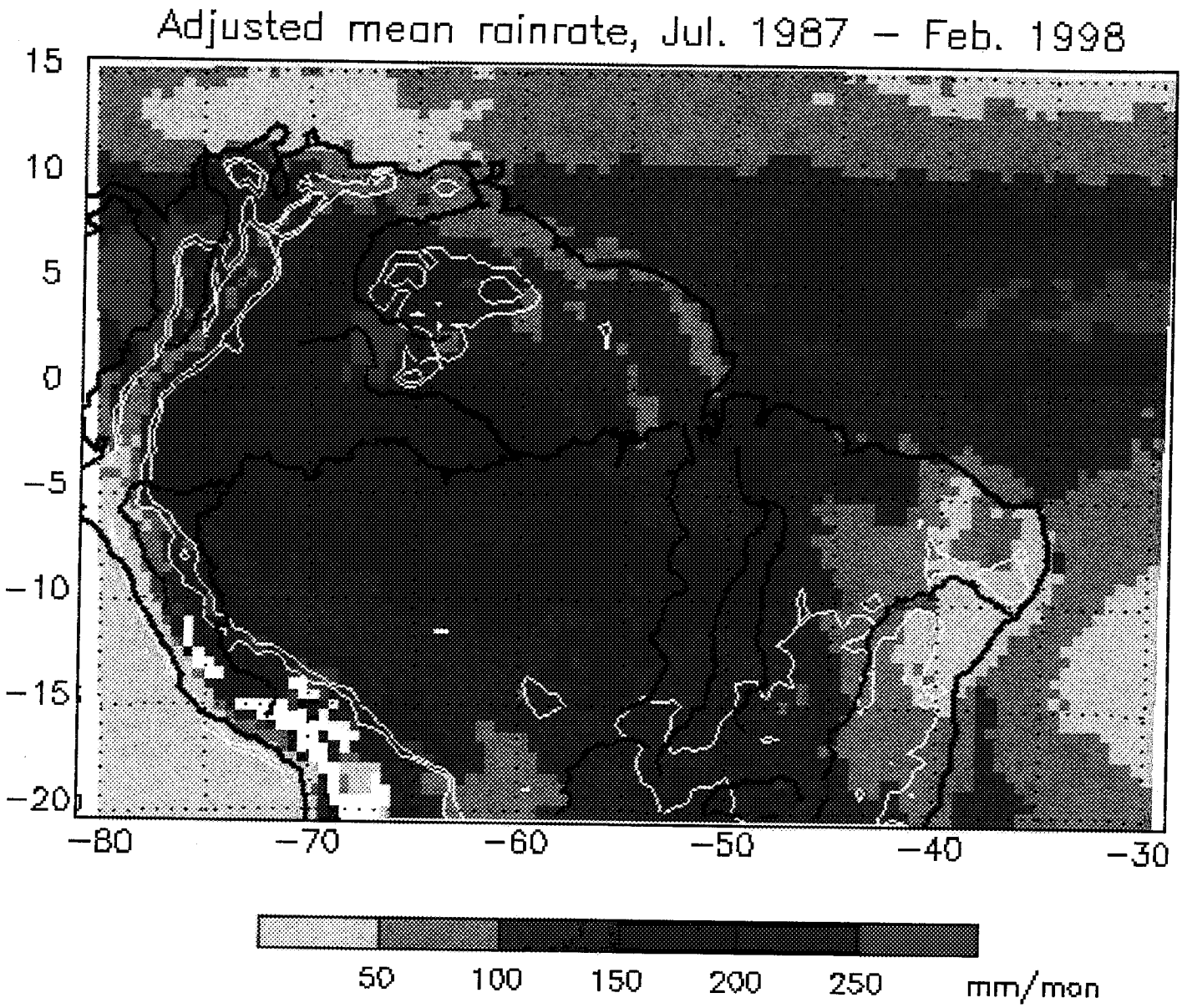
Adjusted mean rainrate, Jul. 1987 – Feb. 1998
15
10
5
0
−5
−10
−15
−20
−80
−70
−60
−50
−40
−30
50
100
150
200
250
mm/mon

Figure 1

A 10-year Climatology of Amazonian Rainfall Derived from Passive Microwave Satellite Observations

A. J. Negri*[1], E. N. Anagnostou[1,2], and R. F. Adler[1]

[1]Laboratory for Atmospheres

NASA/Goddard Space Flight Center, Greenbelt, MD 20771

[2]Universities Space Research Association, Seabrook, MD 20706

9/25/98

Submitted to Journal of Applied Meteorology

* Corresponding author address: Andrew J. Negri,
NASA/GSFC, Code 912, Greenbelt, MD 20771;
email: negri@erin.gsfc.nasa.gov

"A 10-Year Climatology of Amazonian Rainfall Derived From Passive Microwave Satellite Observations"

Andrew J. Negri, Emmanouil N. Anagnostou, and Robert F. Adler

Popular Summary

Rainfall is the most important meteorological variable in the Tropics. The distribution and variability of rainfall has an important societal impact (floods, droughts, and famine). It is also intimately linked to the global atmospheric circulation, since the condensation of water vapor into rainfall is a major heat source that provides the energy for these circulations.

Unfortunately, in the Amazon and across much of South America, rain gages are sparse and weather radar virtually non-existent. This provides the opportunity for satellites to observe and describe the rainfall at high spatial resolution (a regional rainfall climatology). This paper uses data from a series of polar-orbiting satellites to estimate the long term (10+ years) rainfall over Northern South America. The basis for this estimation is as follows: microwave radiation emitted naturally by ocean and land surfaces is intercepted by large water drops and ice particles within raining clouds. Much of this radiation is "scattered" away from the field of view of the satellite's microwave sensors. This results in lower temperatures perceived by these sensors in the presence of raining clouds, as opposed to radiation from clear skies. Thus, the microwave radiation received of the satellite can be estimated to estimate both the presence and intensity of rainfall at the surface. This technique works best for convective clouds (i.e., strong thunderstorms).

Important year-to-year variations (such as El Niño) are observed in the data. Major differences between morning and evening rainfall were found. The effects of topography (mountains, river valleys) and coastlines (land/sea breezes) on the rainfall are documented.

ABSTRACT

In this study we present and describe a satellite-derived, gage-adjusted precipitation climatology over northern South America using a passive microwave technique, the Goddard Profiling Algorithm. A period of data slightly longer than 10 years is examined. The climatologies take the form of the mean estimated (adjusted) rainfall for a 10-year (+) period, with sub-divisions by month and meteorological season. For the six-year period 1992-1997, when two satellites were in operation, diurnal variability (to the extent it is discerned by four unequally spaced observations) is presented. We find an alternating pattern of morning and evening maxima stretching from the northeast (Atlantic coast) clear across the continent to the Pacific. The effects of topography, coastlines and geography (river valleys) on the rainfall patterns are clearly evident. Interannual variability is examined by computing the deviations of yearly and warm-season (DJF) rainfall from their respective long-term means. Interannual variability of the diurnal nature of the rainfall is presented, and the strong El Niño event of 1997-1998 is discussed.

1. Introduction

It has been more than a decade since the launch of the first Special Sensor Microwave/Imager (SSM/I). This passive microwave sensor flies aboard the Department of Defense Meteorological Satellite Program (DMSP), a series of polar-orbiting sun-synchronous meteorological satellites. The long record of data enables us to process and present a 10-year (+) climatology of rainfall derived from the SSM/I observations via application of the Goddard Profiling Algorithm (GPROF). The GPROF (Kummerow et al. 1996) is a physical retrieval technique that produces instantaneous rainfall estimates at 15 km resolution. These estimates are then aggregated into monthly composites and averaged to 0.5° degree resolution. The monthly estimates are adjusted by the technique of Anagnostou et al. (1998), a power-law correction based on the evaluation of the distortion between the probability density functions of the monthly raingage rainfall (the "truth") and the GPROF estimates. This combination of satellite observations and gage measurements produces monthly rainfall fields with small bias, despite the inadequacies of the satellite algorithm and the satellite sampling.

The area of interest in this study is northern South America, specifically the rainforests of Amazonia and the drier coastal regions of Northeast Brazil. The current study extends the work of Negri et al. (1994) who examined warm-season Amazonian precipitation using a scattering-based technique, the Goddard Scattering Algorithm (GSCAT). Over land, GSCAT is nearly identical to full GPROF retrieval. The climatologies presented here take several forms:

a) the mean estimated (adjusted) rainfall for 1987 (July) - 1998 (Feb.) is presented with sub-divisions by month and three-month season;

b) unadjusted estimates are stratified by time of satellite overpass. At least two observations (6/18 LST) are available for the entire period. For the six-year period Jan. 1992 – Nov. 1997, two satellites were in operation, providing up to four observations per day. Diurnal variability (to the extent it is discerned by four unequally-spaced observations) is presented;

c) interannual variability is presented in the form of deviations from the 10-year GPROF mean rainfall, both yearly and for the December through February. Variability of the diurnal character of the rainfall is investigated. The strong El Niño event of 1997-1998 is identified.

The effects of topography and geography (coastlines, river valleys) on the rainfall climatologies are also investigated. Verification using raingages independent of the adjustment procedure is presented.

2. Previous Studies

The most comprehensive study of Amazonian rainfall using *gages* was done by Figueroa and Nobre (1990), who presented both seasonal and yearly analyses using a database of 226 stations with records greater than 7 years. They related the precipitation patterns to average values of the seasonal circulation, and looked at the pronounced effect of topography on the rainfall.

Using three years of three-hourly infrared geosynchronous satellite data, Meiser and Arkin (1987) examined the diurnal cycle of tropical convective cloudiness over the Americas. Among their findings relevant to this study were: 1) there is far more diurnal variance over the continents than oceans; 2) local maxima of diurnal variance were found in areas of strong relief, or where convergent land/sea breezes are common; and 3) there is a pronounced maxima in cloudiness at 1800 LST over the interior of South America during the Austral summer.

Horel et al. (1989) used a 15-year record of outgoing longwave radiation (OLR) to describe the annual cycle of convection that resides over the Amazon Basin during the Austral summer. They found that the onset of the Amazon Basin wet season typically occurs within a single month (sometimes a 5-day period) and that the onset may be blurred by monthly averaged climatologies.

Kousky (1980) investigated the period 1961-70 in Northeast Brazil using surface observations. He found coastal areas to experience a nocturnal maximum in rainfall due to

convergence of on-shore flow and offshore land breeze. He also found that inland (100-300 km) experienced a daytime maximum, associated with the development of and inland advance of the sea-breeze. He found diurnal variability at inland locations to be due to mountain-valley breezes.

Rao et al. (1993) using station data from 1974-83 determined the rainy and dry seasons of eastern Northeast Brazil and examined the link between rainfall there and sea-surface temperatures. Lenters and Cook (1995), using a GCM modeled the regional precipitation climatology of South America. The generation of a thermal low was found responsible for much of the structure of the modeled precipitation, as was the introduction of orography.

Perhaps most relevant to this paper is the work of Garreaud and Wallace (1997) who used nine years of GOES infrared data to define the diurnal march of convective cloudiness over the tropical Americas and surrounding waters. In the process, they favorably compared their infrared results with the microwave-estimated rainfall of Negri et al. (1994). Regional climatologies using passive microwave data are just now coming into the fore. For examples see Negri et al. (1993) for a high resolution climatology of warm-season rainfall over Mexico and the southwest United States and Negri et al. (1994) who examined four regions: the southern United States and Mexico, northern South America, equatorial Africa and the Western Pacific (TOGA-COARE) region.

Much research has also been done on the relationship between large scale precipitation patterns and the El Niño - Southern Oscillation (ENSO). Ropelewski and Halpert (1987) found consistent departures of area-averaged rainfall during ENSO events. Relevant to this study, they

found that the coastal region of Northern South America, from Venezuela east to Brazil, had one of the most consistent ENSO-precipitation relationships of any area studied. Sixteen dry episodes (of 17 ENSO's) were found and the period of deficiency was determined to be from July of the ENSO onset year to March of the following year. This relationship was further quantified in Ropelewski and Halpert (1996). Janowiak and Arkin (1991) observed large-scale shifts in tropical rainfall during the transition from "warm" (1986-87) ENSO conditions to "cold" (1988-89). An area near the mouth of the Amazon River at Belem, Brazil stood out as having a marked difference in mean precipitation between these two periods.

3. Data and methodology

The microwave data used in this study come from the SSM/I instrument onboard the DMSP satellites designated F8, F10, F11 and F13. The SSM/I is a seven-channel passive microwave radiometer with frequencies (in GHz) at 19.35 (H&V), 21.235 (V), 37.0 (H&V), and 85.5 (H&V). Multi-frequency, false-color displays of microwave imagery from the SSM/I may be found in Negri et al. (1989). The satellites are in sun-synchronous, circular (except F10) nearly polar orbits. A complete description of the SSM/I is given in Hollinger et al. (1987). With a swath width of 1400 km, coverage of the entire globe is not possible in a 24 h period. At the equator, monthly sampling of a given point is ~30 observations, subdivided into 15 morning and 15 evening overpasses. The sampling has the potential for introducing both bias and random error into the rain estimates.

Table 1 lists some of the orbit characteristics of each satellite, as well as the period and length of the usable data. Three combinations of the data are also listed in Table 1. Data from the F8/11/13 series constitutes a 95-month (non-continuous) period of up-to-twice-a-day observations. Including observations from F10 extends the period of usable data, but introduces observations approx. 3 h later than the other series. Finally, a 71-month set of common data is available between January 1992 - November 1997, allowing a comparison of mean precipitation at four distinct times.

The rainfall estimates derived herein are produced by the GPROF algorithm (Kummerow et al. 1996), a computationally simple technique for retrieving both precipitation and vertical

hydrometeor profiles. The GPROF is an extension of the original multi-channel retrieval of Kummerow and Giglio (1994). Over land surfaces, GPROF has a greater reliance upon the 85-GHz channel than does the retrieval of Kummerow and Giglio, resulting in estimates largely based on scattering by precipitating ice hydrometeors. GPROF produces instantaneous rainrate estimates at 15 km resolution, which, in this study, are aggregated to monthly totals and averaged to 0.5° grid boxes. The monthly estimates are adjusted to account for the diurnal cycle by the technique of Anagnostou et al. (1998). This correction takes the form of a power-law:

$$GPROF_{adj} = a * (GPROF_{unadj})^{b},$$

where (a,b)=(7.2,0.67) for the 06/18 LST observations and (a,b)=(13.8,0.58) for the 09/21 LST observations. This correction was applied everywhere, but since the adjustment was derived only over land, results over ocean must be viewed qualitatively. A separate aggregation of *unadjusted* estimates by time of satellite overpass was also done. The estimates cover the northern half of South America from 15°N to 20°S and from 80°W to 30°W.

4. Results

a. Mean rainfall

Figure 1 presents the mean GPROF rainfall (mm/mon) during the 107-month period of usable data between July 1987 and February 1998 (see Table 1, combination #2). Contours of topography are displayed at 500 and 1000 m elevations. The significant precipitation maxima that can be discerned are:

- the mean position of ITCZ oceanic rainfall along 5°N from 50°W to 30°W, with a sharp gradient near 10°N;
- the Gulf of Panama, along 78°W from 10°N to the equator (quite possibly one of the rainiest places on the globe);
- a broad maximum in the west-central Amazon Basin;
- a maximum between the Negro and Orinoco Rivers at 2°N, 67°W(the possible result of a mountain/valley circulation as suggested by Kousky, 1980);
- a topographically induced maximum in the mountains of Venezuela (Sierra Pacaraima), near 5°N, 63°W;
- a coastal maximum southeast of the mouth of the Amazon River, near Belem, at 2°S, 48°W;
- an elongated maximum along the eastern slope of the Andes from (10°S, 75°W) to (20°S, 65°W). Note that the maximum along the Andes itself is spurious, a result of occasional misinterpretation by the GPROF of cold (elevated) surface as rainfall. Some, but not all of this spurious rainfall has been eliminated (whitened areas);
- a wide range a north-south movement over land as compared to over ocean.

- the driest regions are found in extreme northeastern Brazil and along the southern Pacific coast.

In Figure 2, we present the adjusted GPROF estimates aggregated by month. Each panel represents the average of 9-10 years of data for that particular month, and includes data from all available satellites. Among the findings are:

- the maximum in the Gulf of Panama (5°N, 78°W) persists virtually year-round but weakens considerably during January to March;
- the oceanic ITCZ progresses from its northernmost position in October southward towards the northeast coast of Brazil in March-April and retreats northward during May;
- a local maximum at the mouth of the Amazon (0°, 50°W) persists during January to May;
- the southern Amazon dries out in the period May to August;
- A pronounced maximum in the Sierra Pacaraima of Venezuela (5°N, 65°W) forms in May and persists through September.

The changes in the areal extent of cold surface in the southern Andes Mts. may be seen as the increased "whitened" area representing ambiguous rain retrieval during the Austral winter months of June through August.

Figure 3 presents the seasonal (3-month) climatology for the combined 06/18 and 09/21 LST series using the meteorological definition of seasons. The December-February period brings the greatest rainfall to the central Amazon, as well as to an elongated area along the eastern slopes of the Andes Mts. The rainfall maximum at Belem, Brazil is most pronounced in March-

May, as is a maximum between the Orinoco River and Negro River near 2°N, 65°W. The topographically induced maximum in the Sierra Pacaraima of Venezuela (5°N, 63°W) is prominent during June-August. Beginning in November, and continuing through February, a broad maximum appears in the highlands of eastern Brazil (Mato Grosso) near 10°S, 50°W. Extreme northeast Brazil is consistently the driest part of that country. This seasonal climatology lends itself to comparison with the gage-derived results of Figueroa and Nobre (1990). In broad terms the agreement is very good, in location, magnitude and orientation of the major features. In fact, the only place where results differ is along the eastern slopes of the Andes (just south of the equator along 78°W) where Figueroa and Nobre found a more pronounced maximum in each season than does the GPROF. This rainfall, most certainly due to upslope flow, might be considered "warm rain" that would be underestimated by a scattering-based technique.

b. Diurnal variation

Figure 4 presents the rainfall climatology by time of satellite overpass for the 71-month period of two-satellite operation, January 1992 to November 1997 (see Table 1, combination #3). Note the unequally-spaced observation times of 06, 09, 18, and 21 LST. The following diurnal features are noted:

- a morning maximum in the Gulf of Panama (5°N, 78°W) maximum, most intense by 09 LST;
- a weak morning maximum offshore in the ITCZ (5°N, 35°W), particularly at 06 LST;

- a morning (both 06 and 09 LST) maximum offshore along the northeast Brazilian coast, including a pronounced signal near the mouth of the Amazon River (0°, 50°W), possibly due to increased convergence in that uniquely shaped region of the coast;
- an 18 LST maximum just on-shore along virtually the entire northern coast of South America. This band moves inland by 21 LST, the likely result of a pronounced sea breeze circulation;
- an 06 LST maximum between the Negro and Orinoco Rivers (2°N, 67°W); possibly related to morning convergence associated with the mountains to the southeast of the maximum;
- an 18 LST maximum in eastern Brazil along the rivers of the Mato Grosso plateau (10°S, 50°W);
- a morning maximum (both at 06 and 09 LST) along the eastern slopes of the Andes mountains.
- an 18 LST maximum between the Negro and Solimoes Rivers around 2°S, 63°W, with a weaker maximum at 09 LST just downriver from their confluence.

This area is examined in greater detail in Figure 5, a blowup of a portion of the Amazon River Basin superimposed with detailed surface hydrology. At 09 LST there is a broad area of 100+ mm/mon rainfall along the main river valley of the Amazon. One finds a minimum (< 50 mm/mon) between the aforementioned the Negro and Solimoes Rivers (3°S, 63°W) and a maximum of 252 mm/mon just south of the river at 3.5°S, 58°W. At 18 LST quite the reverse is true, with a large area of 300+ mm/mon rainfall between the rivers, and an elongated minimum of less than 50 mm/mon downstream. This dry region is also evident at 21 LST. Interestingly, at

18 LST, relative minima are found along the Negro and Solimoes Rivers. This could be the result of a local circulation whereby the cooler river inhibits the convection.

In Figure 6 we attempt to delineate significant diurnal precipitation at each nominal overpass time. By "significant" we simply mean the positive anomaly from the mean, expressed as a percentage of that mean:

$$100*(R_i - R_{tot})/R_{tot} > 0$$

where R_{tot} is the total rainfall and R_i is the rainfall at satellite overpass time "i". This presentation highlights many of the diurnal features listed above. It also highlights the inland propagation of the coastal system between 18 and 21 LST, when it weakens. Evidence of further propagation is evident at 06 LST, with further weakening. Since this is a composite convective line, calculation of the propagation speed would probably not be meaningful. Such calculations for individual squall lines have been done by Garstang et al. (1994).

Another way of looking at the diurnal cycle is presented in Figure 7, by creating the difference between the unadjusted GPROF estimates at 18 LST and 06 LST (top), during the period January 1992-November 1997. The (21 LST – 09 LST) difference is shown in the bottom panel. Cross-section AB is defined for use in Figure 8. The result is an alternating pattern of morning (blue shading) and evening (red shading) maxima stretching from the northeast (Atlantic coast) clear across the continent to the Pacific. The effects of topography, coastlines and river valleys are all evident in this presentation.

Beginning at the northeast coast, the offshore morning (06 and 09 LST) maxima has its afternoon counterpart inland, with apparent propagation of the previous day's rainfall even further inland (the secondary morning maxima roughly paralleling the coast). This alternation is less distinct in central Amazonia, where features related to the distribution of rivers seem to dominate: note the 18 LST maximum at 2°S, 63°W (between the rivers) and the isolated 09 LST maximum just downriver at 2°S, 58°W. On the Pacific coast meanwhile, we find a pronounced afternoon-morning-afternoon sequence at 06 LST as one moves northeastward from the coast. This is related to the mountain/valley circulation of the Andes. The strong circulation of the Gulf of Panama (5°N, 80°W), with its broad oceanic morning maxima and inland afternoon maxima (along the mountains) stands out, with a secondary morning maxima just east of the mountains, southward from 10°N, along 75°W.

In Figure 8 we plot unadjusted GPROF estimates along the cross-section AB in Figure 7, for each of the four satellite overpass times. The values plotted represent the average rainrate over three grid-boxes (1.5°) either side of the line AB. Individual years 1992-97, as well as the 6-year average is shown. A cross-section of topography is shown in the bottom right panel. For the most part, the patterns are consistent from year to year. The largest rainfall signal is clearly associated with the Andes Mountains, but in some years (e.g. during 1993) secondary peaks in the afternoon rainfall over Amazonia and along the northeast are equally important.

c. Interannual variability

In the next several figures we attempt to assess the interannual variability of the analyzed fields. Figure 9 is the adjusted GPROF estimates for individual years minus the mean estimate for the 8-year period 1988-89 and 1992-97. Only data from the F8/11/13 series are used (see Table 1, combination #1), with nominal overpass times of 06 and 18 LST. No estimates were available in 1990-91. Results show the strongest decrease in Amazonian rainfall to be during 1992 and 1997 El Niño events. Increases in precipitation (across virtually all of northern South America) appeared in the La Niña years 1988 and particularly 1989.

In Figure 10 we present the interannual variability of precipitation for the months of December through February (DJF), the beginning of the rainy season in Amazonia. As in Figure 9 we only use data from the 06/18 LST series. No data are available for DJF 1990-91 or DJF 1991-92. In any 3-month estimate near the equator, there are only about 90 samples of data, so some caution should be taken in interpreting the results. Despite this, we find evidence of both the increased DJF precipitation during the La Niña event of 1988-89 and the decrease during the strong El Niño event of 1997-98. Increased rainfall in northern Amazonia was evident in DJF 1995-96 (not an ENSO period). In Figure 11 we contrast the two extrema during the period of data by computing the difference in the gage-adjusted GPROF estimates for DJF 1997-98 and the estimates for DJF 1988-89. The resultant pattern is in agreement with the observational work of Ropelewski and Halpert (1987), particularly their Figure 15, with decreased precipitation in northeast Brazil and increases along the west coast.

In Figure 12 we investigate the interannual variability of the diurnal nature of the precipitation. We display the difference between the 18 LST and 06 LST unadjusted estimates for the same years as in Figure 9. At first glance, very little variability is detected; the patterns tend to repeat from year to year. The most consistent areas are the Gulf of Panama, the slopes of the Andes Mts. and the central and eastern portions of Brazil. It is only along the north and northeast coasts of South America do we find pronounced interannual variability. Note for example the strong diurnal character along the northeast coast in 1988 and 1989 (La Niñas) and the weakened circulation in 1992 and 1997 (El Niños). The morning maximum offshore of the northeast Brazilian coast virtually disappears during 1997.

d. Verification

A scatter-plot of GPROF gage-adjusted estimates versus monthly raingage observations over the Amazon Basin is shown in Figure 13. Plotted data include gages from both the Amazon and eastern Brazil (state of Ceara) during 1992-97. The Ceara data set is independent of the adjustment procedure. The plot shows that the overall bias of the adjusted GPROF estimates are close to zero, and are highly correlated (0.84) with the independent gages. Considerable scatter still exists at rainrates above 200 mm/mon. The root-mean-square-error is 28.2% of the mean, a low value considering we are using point, not area-averaged, rainfall measurements.

5. Summary and Conclusions

In this study we presented and described a satellite-derived, gage-adjusted precipitation climatology over northern South America using a microwave technique, the Goddard Profiling Algorithm, adjusted by the gages. A period of data slightly longer than 10 years was examined. The climatologies took the form of the mean estimated (adjusted) rainfall for a 10-year (+) period, with sub-divisions by month and meteorological season. For the six-year period 1992-1997, when two satellites were in operation, diurnal variability (to the extent it is discerned by four unequally spaced observations) was presented. Interannual variability (i.e. deviations from the 10-year GPROF mean rainfall) was presented as both yearly and seasonal (DJF) deviations, and included the strong El Niño event of 1997-1998. Specific findings included:

- a preference for morning oceanic rainfall (ITCZ), notably at 06 LST;
- a rainfall maximum in the Gulf of Panama, exclusively a morning phenomenon, and most intense at 09 LST. With estimated rainfall in excess of 3 m, this is probably one of the wettest spots on the planet. This features is evident 9 months of the year;
- a broad maximum in the west-central Amazon Basin, maximized at 18 LST;
- an elongated (morning) maximum along the eastern slopes of the Andes Mts.;
- a persistent local maximum at the mouth of the Amazon during January to May, due to increased convergence in that uniquely shaped region of the coast;
- an 18 LST maximum along virtually the entire on-shore side of the northern coast of South America. This moves inland by 21 LST, the apparent result of a pronounced sea breeze

circulation; attendant to this is a morning (both 06 and 09 LST) maximum offshore along the northeast Brazilian coast.

Several rainfall maxima are the apparent results of local circulations as suggested by Kousky (1980):

- a maximum between the Negro and Orinoco Rivers at 2°N, 67°W, the possible result of a mountain/valley circulation;
- a topographically induced maximum in the mountains of Venezuela (Sierra Pacaraima), near 5°N, 63°W from May through September;
- an 06 LST maximum between the Negro and Orinoco Rivers;
- an 18 LST maximum between the Negro and Solimoes Rivers, where they come together to form the Amazon River. There is a suggestion of a weak 09 LST maximum just downriver from this confluence;
- an 18 LST maximum in eastern Brazil along the rivers of the elevated Mato Grosso plateau.

The interannual variability of the GPROF precipitation estimates was assessed. Increased precipitation during DJF was evident during the La Niña event of 1988-89 and decreases appeared during the strong El Niño event of 1997-98. Increased rainfall in northern Amazonia was evident in DJF 1995-96 as well, a year with little ENSO signal. Diurnal variation was stronger (weaker) in the El Niño (La Niña) years. Validation of the monthly GPROF estimates was performed using quasi-independent rain gages. The gage-adjusted estimates had bias close to zero, and were highly correlated (0.84) with the gages. Considerable scatter existed at rainrates above 200 mm/mon. The root-mean-square-error was 28.2% of the mean.

Future work will encompass the creation of an infrared technique tuned to the instantaneous microwave results that will allow the full diurnal cycle to be resolved.

Acknowledgement. The authors wish to thank Dr. George Huffman for his critical review of the manuscript.

References

Anagnostou, E. N., A. J. Negri, and R. F. Adler, 1998: Adjustment of monthly microwave estimates over Amazonia. *J. Appl. Meteor.* (submitted).

Figueroa, S. N. and C. A. Nobre, 1990: Precipitation distribution over central and western tropical South America. *Climanálise*, **5**, 36-47.

Garreaud, R. D. and J. M. Wallace, 1997: The diurnal march of convective cloudiness over the Americas. *Mon. Wea. Rev.*, **125**, 3157-3171.

Garstang, M., H. L. Massie, Jr., J. Halverson, S. Greco, and J. Scala, 1990: Amazon coastal squall lines. Part I: Structure and kinematics. *Mon. Wea. Rev.*, **122**, 608-622.

Hollinger, J., R. Lo, G. Poe, R. Savage, and J. Peirce, 1987: Special Sensor Microwave/Imager User's Guide. Naval Research Laboratory, Washington, DC, 177 pp.

Horel, J. D., A. N. Hahmann, and J. E. Geisler, 1989: An investigation of the annual cycle of convective activity over the Tropical Americas. *J. Climate*, **2**, 1388-1403.

Janowiak, J. E. and P. A. Arkin, 1991: Rainfall variations in the tropics during 1986-1989 as estimated from observations of cloud-top temperature. *J. Geophys. Res.*, **96**, 3359-3373.

Kousky, V. E., 1980: Diurnal rainfall variation in Northeast Brazil. *Mon. Wea. Rev.*, **108**, 488-498.

Kummerow, C. and L. Giglio, 1994: A passive microwave technique for estimating rainfall and vertical structure information from space, Part I: algorithm description. *J. Appl. Meteor.*, **33**, 3-18.

Kummerow, C., W. S. Olson, and L. Giglio, 1996: A simplified scheme for obtaining precipitation and vertical hydrometeor profiles from passive microwave sensors. *IEEE Trans. Geosci. Remote Sensing*, **34**, 1213-1232.

Lenters, J. D. and K. H. Cook, 1995: Simulation and diagnosis of the regional summertime precipitation climatology of South America. *J. Climate,* **8**, 2988-3005.

Meisner, B. N. and P. A. Arkin, 1987: Spatial and annual variations in the diurnal cycle of large-scale tropical convective cloudiness and precipitation. *Mon. Wea. Rev.*, **115**, 2009-2032.

Negri, A. J., R. F. Adler, and C. D. Kummerow, 1989: False-color display of Special Sensor Microwave/Imager (SSM/I) data. *Bull. Amer. Meteor. Soc.*, **70**, 146-151.

Negri, A. J., R. F. Adler, R. A. Maddox, K. W. Howard, and P. R. Keehn, 1993: A regional rainfall climatology over Mexico and the southwest United States derived from passive microwave and geosynchronous infrared data. *J. Climate*, **6**, 2144-2161.

Negri, A. J., R. F. Adler, E. J. Nelkin, and G. J. Huffman, 1994: Regional rainfall climatologies derived from Special Sensor Microwave Imager (SSM/I) data. *Bull. Amer. Meteor. Soc.*, **75**, 1165-1182.

Rao, V. B., M. C. deLima, and S. H. Franchito, 1993: Seasonal and interannual variations of rainfall over eastern Northeast Brazil. *J. Climate*, **6**, 1754-1763.

Ropelewski, C. F. and M. S. Halpert, 1987: Global and regional scale precipitation patterns associated with the El Niño /Southern Oscillation. *Mon. Wea. Rev.*, **115**, 1606-1626.

Ropelewski, C. F. and M. S. Halpert, 1996: Quantifying Southern Oscillation precipitation relationships. *J. Climate* , **9**, 1043-1059.